Am J Transl Res 2018;10(5):1357-1372
www.ajtr.org /ISSN:1943-8141/AJTR0072335

Original Article

Targeting CAND1 promotes caspase-8/RIP1-dependent apoptosis in liver cancer cells

Zhihui Che[1], Fuchen Liu[1,2], Wenli Zhang[1], Mary McGrath[3], Daisen Hou[1], Ping Chen[1], Chunhua Song[3], Dongqin Yang[1]

[1]Department of Digestive Diseases of Huashan Hospital, Fudan University, Shanghai 200040, China; [2]The Third Department of Hepatic Surgery, Eastern Hepatobiliary Surgery Hospital, Second Military Medical University, Shanghai 200438, China; [3]Department of Pediatrics, Pennsylvania State University College of Medicine, Hershey 17033, PA, USA

Received January 5, 2018; Accepted February 23, 2018; Epub May 15, 2018; Published May 30, 2018

Abstract: Cullin-associated NEDD8-dissociated 1 (CAND1) plays a vital role in regulating the activity of Cullin-RING ubiquitin ligases (CRLs), which are frequently dysregulated in cancer. However, the role of CAND1 in hepatocellular carcinoma (HCC) remains unknown. Here, we found that CAND1 was overexpressed in HCC tissues compared to corresponding adjacent liver tissues (71.7% vs 16.7%); high expression of CAND1 was associated with poor overall survival (40.7 vs 57.3 months, P=0.0013); and CAND1 was an independent risk factor for the prognosis of HCC patients (N=138, P=0.018). Functional studies revealed that CAND1 knockdown efficiently suppressed the proliferation of liver cancer cells by activating caspase-8-dependent mitochondrial apoptosis. We also observed a mutual activation loop between caspase-8 and Receptor Interacting Protein 1 (RIP1), which amplified CAND1 knockdown-induced apoptotic signals in the cells. Furthermore, RIP1 inhibitor Necrostatin-1 eliminated the activation of caspase-8. In conclusion, our study pioneered in reporting high CAND1 expression as a predictor of poor prognosis for HCC patients. CAND1 silencing suppressed HCC cell proliferation by inducing caspase-8/RIP1-dependent apoptosis. These findings supported that CAND1 could be a new therapeutic target for liver cancer.

Keywords: Cullin-associated NEDD8-dissociated 1 (CAND1), hepatocellular carcinoma (HCC), apoptosis, caspase-8, Receptor Interacting Protein 1 (RIP1)

Introduction

Cullin-RING ligases (CRLs) share a similar structure model in which Cullin acts as a molecular scaffold binding a substrate recognition subunit (SRS) at the N-terminus and a RING protein at the C-terminus [1]. CRLs are the largest group of E3 ubiquitin ligases and account for the ubiquitination of nearly 20% of cellular proteins doomed for degradation via proteasomes [2]. CRLs highlight their role in regulating various biological processes including cell cycle progression, gene transcription, apoptosis, signal transduction and DNA replication. Dysregulation of CRLs is associated with many diseases, including cancers, suggesting that CRLs could be potential anti-cancer targets [3, 4].

It is well characterized that CAND1 is involved in the general dynamic regulation of CRLs repertoire [5]. The activity of CRL E3 ligases is largely dependent on Cullin neddylation, whereby a covalent modification of Cullin with the ubiquitin-like protein NEDD8 will induce the conformational rearrangement of Cullin and further promote the ubiquitination of substrates [6]. Once NEDD8 is unconjugated from Cullin, which is catalyzed by COP9 signal some (CSN), CAND1 will interact with and sequester the unneddylated Cullin. This allows SRS part exchange followed by reactivation of the assembled CRL [7]. The Cullin neddylation cycle has attracted much attention in cancer therapy [8, 9]. For example, MLN4924, the first potent small molecule inhibitor of the NEDD8-activating enzyme, inactivates the entire CRLs by blocking Cullin neddylation, and has been advanced to several Phase I clinical trials against human malignancies [10, 11].

In this study, we revealed the correlation between CAND1 expression and clinical pathological

features of HCC patients and found that CAND1 plays a key role in proliferation of liver cancer cells. We uncovered a positive mutual activation loop between caspase-8 and RIP1 which amplified the apoptotic signals of CAND1 knockdown in HCC cells. Our data suggested that CAND1 might serve as a potential biomarker for prognosis and a promising target for therapy in liver cancer.

Materials and methods

Patients and clinical tissue samples

A total of 223 primary HCC samples were obtained from patients who underwent surgical resection at Eastern Hepatobiliary Surgery Hospital, the Second Military Medical University, Shanghai, China. All tissues were obtained before chemical, radiation, and other anti-cancer therapy. The diagnosis of HCC was made based on the postoperative pathology evaluation. Prior written informed consents from all patients and the approval from the Ethics Committee of Eastern Hepatobiliary Surgery Hospital were obtained. The postoperative pathological data was obtained from the hospital medical records and has been followed-up for 8 years. Overall survival (OS) was calculated from the date of surgery to the date of death or the last follow-up. Relapse free survival (RFS) was defined as the interval time between the surgery and recurrence date. Among the samples, 63 pairs of tumor tissues and their corresponding adjacent liver tissues were used for Western Blot analysis of CAND1 expression, and another 22 liver tissues were used for Western Blot to further analyze the correlation of CAND1 and RIP1; 138 pairs of tumor tissues and their corresponding adjacent liver tissues were used for Immunohistochemistry analysis.

Immunohistochemistry (IHC) analysis

The paraffin embedded tissues excised from the 138 HCC patients were used to construct tissue microarrays. Immunohistochemistry was performed as previous described [12, 13]. Briefly, tissue microarrays were deparaffinized in xylnen, rehydrated through graded ethanol, and heat treated in citrate buffer (30 min, PH 6.0, Dako, Carpinteria, CA, USA) for antigen retrieval. 3% H_2O_2 was used to block the activity of endogenous peroxidase. The microarrays were blocked with 5% non-fat milk diluted in Tris-buffered saline-Tween 20 (TBST) for 2 hours followed by incubation with primary antibody overnight. Next, the microarrays were incubated with the secondary antibody (Dako, Carpinteria, CA, USA) for 2 hours before they were stained with hematoxylin using a Dako Envisions kit (Dako, Carpinteria, CA, USA). Based on the percentage of positive-staining cells, and the staining intensity, four random views (400 times of magnification) were adopted to assess the protein expression level with the Aperio ScanScope™ software, and scored by two pathologists with a blinded method. The percentage of positive-staining cells were scored 1 (0 to 25%), 2 (26 to 50%), 3 (51 to 75%), or 4 (76 to 100%). The staining intensity was scored as 1 (negative staining), 2 (weak staining), 3 (moderate staining), or 4 (strong staining). The composite score was obtained by multiplying the percentage grade by the intensity score and classified into four groups: 0-1 represents +, 2-4 represents ++, 5-8 represents +++, 9-12 represents ++++. Subjects were allocated into high (+++ and ++++) or low (+ and ++) CAND1 expression and the clinical features were compared between the two groups as we previously reported [12-14].

Cell culture and reagents

Human immortalized liver cell lines LO2, MIHA, and liver cancer cell lines SMMC7721, Huh7, Hep3B, Li7, BEL-7404 were purchased from the Type Culture Collection of Chinese Academy of Sciences, Shanghai, China; liver cancer cell line LM6 was obtained from the Liver Cancer Institute, Zhongshan Hospital, Fudan University, Shanghai, China. Cells were cultured in Dulbecco's Modified Eagle's Medium (DMEM) (Gibco, Gaithersburg, MD, USA) supplemented with 10% fetal bovine serum (FBS) (Thermo Fisher Scientific, Waltham, USA) and 1% penicillin-streptomycin at 37°C with 5% CO_2.

Necrostatin-1 (S8037) and Z-VAD-fmk (S7023) were purchased from Selleck, Shanghai, China.

Small interfering RNA (siRNA) and transient transfection

RNA interference assay was performed as previous described [12, 15]. The siRNAs were synthesized at RiboBio Co, Ltd., Guangzhou, China. Cells were split 18 hours before transfection. siRNAs were transfected into the cells at a concentration of 100 nmol/L with Lipofectamine™-RNAimax (Invitrogen, Carlsbad, CA, USA). The

sequence of the scrambled siRNA is 5'-TTCTCCGAACGTGTCACGTTT-3'. The sequences of CAND1 siRNAs are as follow: seq-1: 5'-CGUGCAACAUGUACAACUA-3'; seq-2: 5'-GACUUUAGGUUUAUGGCUA-3'; seq-3: 5'-CAACAAGAACCUACAUACA-3'. The sequence of caspase-8 siRNA is 5'-UGGAUUUGCUGAUUACCUA-3'.

Immunoblotting

The protein concentration of the cell extracts was quantified using an enhanced BCA Protein Assay Kit (Beyotime Biotechnology, Nantong, China). Protein samples (30 ug) were separated by 12% sodium dodecyl sulfate-polyacrylamide gel electrophoresis (SDS-PAGE) and then transferred to 0.45 um polyvinylidine difluoride filter (PVDF) membranes (Millipore, Billerica, MA, USA). The membrane was blocked with 5% nonfat milk diluted by TBST for 2 hours and then incubated with primary antibodies at 4°C overnight. Next, the membrane was washed with TBST three times, and probed with HPR-linked secondary antibodies for 2 hours at room temperature. An enhanced chemiluminescence detection kit (Sangon Biotech, Shanghai, China) was used to visualize the proteins bands. The signal intensity of indicated proteins was obtained with a densitometric analysis using the software of Image J (NIH, Bethesda, Maryland, USA) as we previously reported [12, 15]. β-actin was used as a loading control to quantify the expression level of indicated proteins.

Antibodies of cleaved-PARP (5625S), cleaved-caspase-8 (9496), cleaved-caspase-9 (7237S), RIP1 (3493), Bcl-2 (2872), Mcl-1 (5453S), Bax (5023), Bak (6947P), Bid (2002), Cytochrome C (11940), Goat-α-Rabbit (7074) and Goat-α-Mouse (7076) were purchased from Cell Signaling Technology Inc, Danvers, MA, USA; AIF (1020-S), VDAC-1 (7237S) and β-Tubulin (1897-1) were purchased from Epitomics, Burlingame, CA, USA; β-Actin (CW0096M) was purchased from CWBiotech, Beijing, China; MLKL (CY5493) was purchased from Abways, Shanghai, China; and CAND1 (H00055832-M01) was purchased from Abnova, Taiwan.

Cell proliferation assay

Cell proliferation was measured using CellTiter 96® AQ_{ueous} One Solution Cell Proliferation Assay (MTS) (G3580, Promega, Madison, WI, USA). Briefly, cells (2000 cells/well) transfected with CAND1 siRNA (siCAND1) or control scramble siRNA (siNC) were seeded in 96-well plates in triplicate for a different number of days. A 120 ul mixture of fresh DMEM (supplemented with 10% FBS, 100 ul) and MTS (20 ul) was added to each well, and incubated for another 2 hours at 37°C, according to the manufacturer's instructions. The OD450 of each well was tested by Infinite200Pro (Tecan, Shanghai, China), and the percent cell viability was compared to the siNC control. The data were analyzed and graphed with the Graphpad Prism 6.0 software [12, 15].

Hoechst33342 staining

Cells were split in 6-well plates (1×10^5 cells/well) and transfected with CAND1 siRNA (siCAND1) or control scramble siRNA (siNC). 96 hours after transfection, cells were washed with PBS twice, stained with Hoechst33342 (10 ug/ml, Beyotime Biotechnology, Nantong, China) for 15 minutes at room temperature, and photographed under a fluorescence microscope (Leica, Wetzlar, Germany) at emission wavelength of 460nm and excitation wavelength of 346 nm. The fluorescence intensity was quantified using the software of Image J (NIH, Bethesda, Maryland, USA) as we previously reported [14].

Cell cycle distribution analysis

Cells were treated with CAND1 siRNA (siCAND1) or scramble siRNA (siNC) for the indicated days. Cells were harvested and fixed in 70% ethanol at -20°C overnight, and stained with propidium iodide (36 ug/ml, Sigma) containing 400 ug/ml RNase (Roche). They then underwent shaking for 30 minutes on ice. Then, cells were collected and analyzed by flow cytometry (CyAn™ ADP, Beckman Coulter, Brea, CA, USA) for cell cycle profile and apoptosis analysis. The data was analyzed with the software of ModFit LT as we previously reported [12, 15].

Apoptotic assay

The apoptotic cells were determined by flow cytometry using the Annexin V-FITC and PI Apoptosis Detection Kit following the manufacturer's instructions. Briefly, 3×10^5 cells were treated with CAND1 siRNA (siCAND1) or scramble siRNA (siNC) for indicated days. The cells were then harvested, washed with PBS and incubated with Annexin V-FITC and PI for staining in binding buffer at room temperature for 15 minutes in the dark. The stained cells were flowed

using the CyAn™ ADP instrument (Beckman Coulter, Brea, CA, USA) and analyzed with the FlowJo v10.0.6 software [12, 15].

Quantification of cleaved caspase-3

Cells were treated with CAND1 siRNA (siCAND1) or control scramble siRNA (siNC) for 96 hours. To measure the cleavage of caspase-3, cells were harvest and washed with PBS and then incubated with FITC-DEVD-FMK (BioVision, Milpitas, CA, USA) in PBS at 37°C and 5% CO_2 for 30 minutes. Cells were collected by centrifugation at 3000 r.p.m., re-suspended in wash buffer and centrifuged twice. After re-suspension in PBS, samples were subjected to flow cytometry analysis with CyAn™ ADP. Capase-3 cleavage was analyzed with the FlowJo v10.0.6 software as we previously reported [15].

Detection of reactive oxygen species (ROS)

The intracellular reactive oxygen species (ROS) were detected using 2', 7'-dichloro-fluorescein diacetate (DCFH-DA) as a probe. ROS were detected with a Reactive Oxygen Species Assay Kit (Beyotime) according to the manufacturer's instructions as we previously reported [15, 16]. Briefly, cells were treated with CAND1 siRNA (siCAND1) or scramble siRNA (siNC) for a different number of days. The cells were harvested, washed twice with PBS, and then incubated with 10 μM DCFH-DA (S0033, Beyotime Biotechnology, Nantong, China) diluted in PBS at 37°C for 20 minutes for whole cell ROS detection; or incubated with 5 μM MitoSOX Red mitochondrial superoxide indicator (40778ES50, Yeasen, Shanghai, China) at 37°C for 10 minutes for mitochondrial-specific ROS detection. The formation of the fluorescent-oxidized derivative of DCFH-DA or MitoSOX Red was monitored using CyAn™ ADP at an emission wavelength of 525 or 580 nm, and an excitation wavelength of 488 or 510 nm, and analyzed with the FlowJo v10.0.6 software.

Detection of mitochondrial membrane potential (MMP)

Cells were treated with CAND1 siRNA (siCAND1) or scramble siRNA (siNC) for the indicated days in 6-well plates, and $\Delta\Psi$ (MMP collapse) was analyzed by JC-1 staining according to the manufacturer's instructions as we previously reported [15]. The dye JC-1 can exist as a monomer or as JC-1 aggregates (J-aggregates), giving green (510-530 nm) and red (650 nm) fluorescence emissions respectively. For flow cytometry, cells were collected and then washed once with PBS. The pellets were re-suspended with normal medium containing 5 ug/ml JC-1. After incubation for 20 minutes at 37°C in 5% CO_2, the cells were immediately centrifuged to remove the supernatant, washed twice with PBS, re-suspended in PBS, and then analyzed by flow cytometry at an excitation wavelength of 488 nm. The percentage of green fluorescence from the JC-1 monomers was used to represent the cells that lost $\Delta\Psi$.

Mitochondria isolation

Mitochondria isolation was performed as previous described [15]. The mitochondria isolation kit (C3601, Beyotime Biotechnology, Nantong, China) was used according to the manufacturer's protocol. Mitochondrial and cytoplasm fractions isolated by gradient centrifugation were then subjected to immunoblotting analysis. Loading controls of the subcellular components are: Voltage-Dependent Anion Channel 1 (VDAC1) for the mitochondrial fraction, and β-Tubulin for the cytoplasm fraction.

Statistical analysis

The statistical significance of differences between groups was assessed using the software of GraphPad Prism 6 and SPSS 22.0. The unpaired two-tailed t-test was used for the comparison of parameters between two groups. Categorical data were analyzed by the Pearson's chi-square or Fisher's exact tests. Correlation between protein expression and clinic-pathological features was performed by the two tailed Mann-Whitney U-test or Kruskal-Wallis test. Survival curves were plotted by the Kaplan-Meier method and statistical differences were analyzed using the log-rank test. Cox's proportional hazards regression model was adopted to analyze independent prognostic factors. For all the tests, three levels of significance (*, $P<0.05$; **, $P<0.01$; and ***, $P<0.001$) were used.

Results

Expression of CAND1 in human liver cancer and its correlation with patients' clinical features

To understand the clinical significance of CAND1, we analyzed its expression in human liver cancer. Western Blot assays of 63 pairs of liver

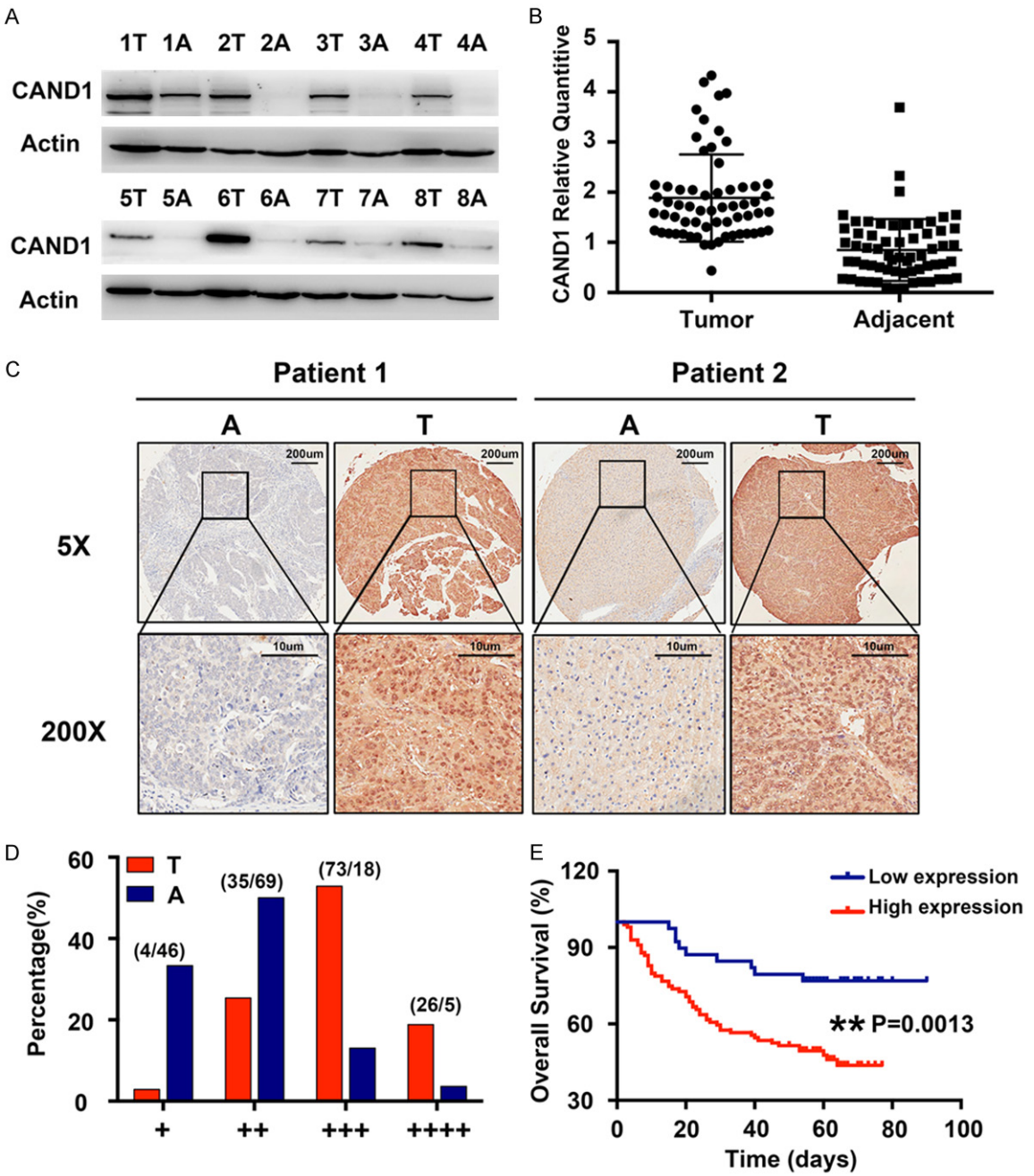

Figure 1. CAND1 expression in liver cancer tissues and its correlation with patient survival. (A, B) Representative western blot bands of CAND1 expression in liver cancer and corresponding adjacent tissues (8 of 63 pairs). β-actin was used as a loading control. T: tumor tissue; A: adjacent tissues (A). Dot Chart showed the relative CAND1 expression detected by western blot in 63 pairs of liver cancer tissues and adjacent tissues. The signal intensity of indicated proteins was obtained with a densitometric analysis using the software of Image J (MD, USA). β-actin was used as a loading control (B). (C) Representative photomicrographs showing IHC staining of CAND1 in liver cancer and corresponding adjacent tissues of two patients. T: tumor tissue; A: adjacent tissues. Magnification ×5 and ×200. (D) The cartogram depicts the distribution of CAND1 expression based on IHC staining intensity from the weakest (+) to the strongest (++++) in 138 cases of HCC tumor tissue (T) compared to that of adjacent tissues (A). (E) Kaplan-Meier log-rank survival analysis in the patients with CAND1 high expression [IHC staining (+++) or (++++)] compared to that of low expression [IHC staining (+) or (++)]. Mean ± SD, **P<0.01.

cancer tissues and the corresponding adjacent liver tissues indicated that CAND1 was overexpressed in human liver cancer (**Figure 1A** and **1B**). IHC staining of tissue arrays (138 HCCs

Table 1. Clinical characteristics of 138 HCC patients and CAND1 expression

Factors	Expression of CAND1		*P* Value
	Low (n=39)	High (n=99)	
Sex			
Male	36	88	0.533
Female	3	11	
Age, years			
<50	15	42	0.673
≥50	24	57	
Child-Pugh score			
A/B	35	89	0.978
C	4	10	
AFP, ng/ml			
≤20	15	30	0.361
>20	24	69	
HBeAg			
Negative	32	83	0.802
Positive	7	16	
Tumor differentiation			
I/II	7	5	0.015
III/IV	32	94	
Tumor size, cm			
<5	25	34	0.001
≥5	14	65	
Tumor number			
Single	29	73	0.941
Multiple	10	26	
Satellite opacities			
No	11	22	0.462
Yes	28	77	
Microvascular thromboembolism			
No	16	33	0.399
Yes	23	66	
Survival time, years			
<5	21	81	0.001
≥5	18	18	
Recurrence-free survival time, years			
<5	28	80	0.251
≥5	11	19	

P<0.05 was considered statistically significant. Pearson's chi-square test was used. Abbreviation: AFP, alpha fetoprotein; HBeAg, hepatitis Be antigen.

were included) further indicated the tendency of high expression of CAND1 in liver cancer (**Figure 1C**). The samples were classified into four groups according to the staining intensity from the weakest (+) to the strongest (++++). For the tumor tissues, there were 39 cases that had low intensity of CAND1 staining (4/138, +; 35/138, ++), classified as low expression; and 99 cases showed high intensity of CAND1 staining, classified as high expression (73 /138, +++; 26/138, ++++). While for the adjacent liver tissues, 115 cases had low expression (46/ 138, +; 69/138, ++) and 23 cases presented with high expression of CAND1 (18/138, +++; 5/138, ++++) (**Figure 1D**). The mRNA level of CAND1 matched the high expression in liver cancer seen in cohorts from the ONCOMINE database [fold change=1.528, P<0.001, liver (n=220) vs HCC (n=225)].

A clinical and pathology association study of these 138 HCCs found that overexpression of CAND1 was associated significantly with larger tumor size (P=0.001) and poorer differentiation (P= 0.015); and was not associated with metastasis and invasion, as judged by tumor numbers, satellite opacities, and microvascular thromboembolism (Pearson's Chi-square test, **Table 1**). More intriguingly, overexpression of CAND1 was correlated significantly with poorer overall survival (median survival: 40.7 vs 57.3 months, P=0.0013, **Figure 1E**). Cox proportional hazard regression analysis indicated that high CAND1 expression was an independent prognostic factor for overall survival of HCC patients (P=0.018, **Table 2**).

Taken together, these results indicated that CAND1 was highly expressed in liver cancer tissues, and the patients with higher CAND1 expression had a poorer clinical outcome.

CAND1 knockdown selectively suppressed proliferation of liver cancer cells

CAND1 was found by western blot assays to be highly expressed in liver cancer cell lines (Hep3B, Li7, 7404, Huh7, SMMC7721 and LM6) compared to immortalized liver cell lines (LO2,

Table 2. Uni- and multivariate analysis of factors associated with survival in 138 HCCs

OS					
Factors	Univariate	Multivariate			
	P	B	Exp (B)	95% CI	P
HBeAg (negative vs positive)	0.099				NS
Serum AFP, ng/ml (≤20 vs >20)	0.382				NA
Tumor differentiation (I/II vs III/IV)	0.046				NS
Tumor size, cm (≤5 vs >5)	0.002	-0.749	0.473	0.271-0.823	0.008
Tumor number (single vs multiple)	0.139				NS
Microvascular invasion (no vs yes)	0.249				NA
Satellite opacities (no vs yes)	0.807				NA
CAND1 expression (low vs high)	0.006	-0.828	0.437	0.220-0.867	0.018
RFS					
Factors	Univariate	Multivariate			
	P	B	Exp (B)	95% CI	P
HBeAg (negative vs positive)	0.054	0.56	1.75	1.039-2.950	0.036
Serum AFP, ng/ml (≤20 vs >20)	0.353				NA
Tumor differentiation (I/II vs III/IV)	0.027	-1.148	0.317	0.099-1.020	0.05
Tumor size, cm (≤5 vs >5)	0.008	-0.504	0.604	0.383-0.952	0.03
Tumor number (single vs multiple)	0.054				NS
Microvascular invasion (no vs yes)	0.454				NA
Satellite opacities (no vs yes)	0.692				NA
CAND1 expression (low vs high)	0.142				NS

Cox's proportional hazards regression model. Abbreviation: OS, overall survival; RFS, relapse free survival; NA, not adopted; NS, not significant; AFP, alpha fetoprotein; HBeAg, hepatitis Be antigen; 95% CI, 95% confidence interval.

MIHA) (**Figure 2A**). With the knowledge that CAND1 was highly expressed in liver cancer tissues, we assumed that CAND1 may be involved in HCC tumorigenesis. To confirm our hypothesis, we observed the effect of CAND1 silencing on liver cancer cells. **Figure 2B** showed that three different CAND1 siRNAs sequences effectively confined CAND1 expression (**Figure 2B**). MTS colorimetric assay revealed that siRNA sequence-1 inhibited the growth of SMMC7721 the most (**Figure 2C**). Moreover, CAND1 siRNA (siCAND1) significantly suppressed the proliferation of Huh7 and LM6 tumor cells compared to that of scramble siRNA control (siNC) (**Figure 2D** and **2E**), but the growth-inhibitory effect of siCAND1 on immortalized liver cell lines LO2 and MIHA had no significant difference compared to that of siNC (**Figure 2F** and **2G**). The effect of siCAND1 on cell proliferation suppression was also observed under the fluorescence microscope with hoechst33342 staining in SMMC7721 and LM6 tumor cells. The quantitation data showed there was a significant decrease in intensely staining cells in the siCAND1 group compared to that of the siNC group. (**Figure 2H**).

CAND1 knockdown suppressed cell proliferation by activating mitochondrial apoptosis signals in HCC cells

To understand the mechanism underlying CAND1 knockdown-induced suppression of cell proliferation, the cell cycle profile was explored in SMMC7721 cells. G2/M phase arrest and apoptotic sub-G1 proportions were increased following CAND1-silencing (siCAND1) treatment compared to the control siNC over the treatment days. The quantitative data showed that siCAND1 treatment for 96 hours significantly increased the percentage of both apoptotic cells and G2/M phase cells in the tumor cells compared to that of the control groups (**Figure 3A**), suggesting that the increased cell growth inhibition was owing to enhanced apoptosis. An Annexin V and PI double staining assay was then conducted to further analyze the apoptotic effect of CAND1-silencing on LM6 cells. The total percentage of cells that underwent early apoptosis [Annexin V (+) and PI (-)] and late apoptosis [Annexin V (+) and PI (+)] were counted. siCAND1 treatment showed an increased number of cells undergoing apoptosis proportional-

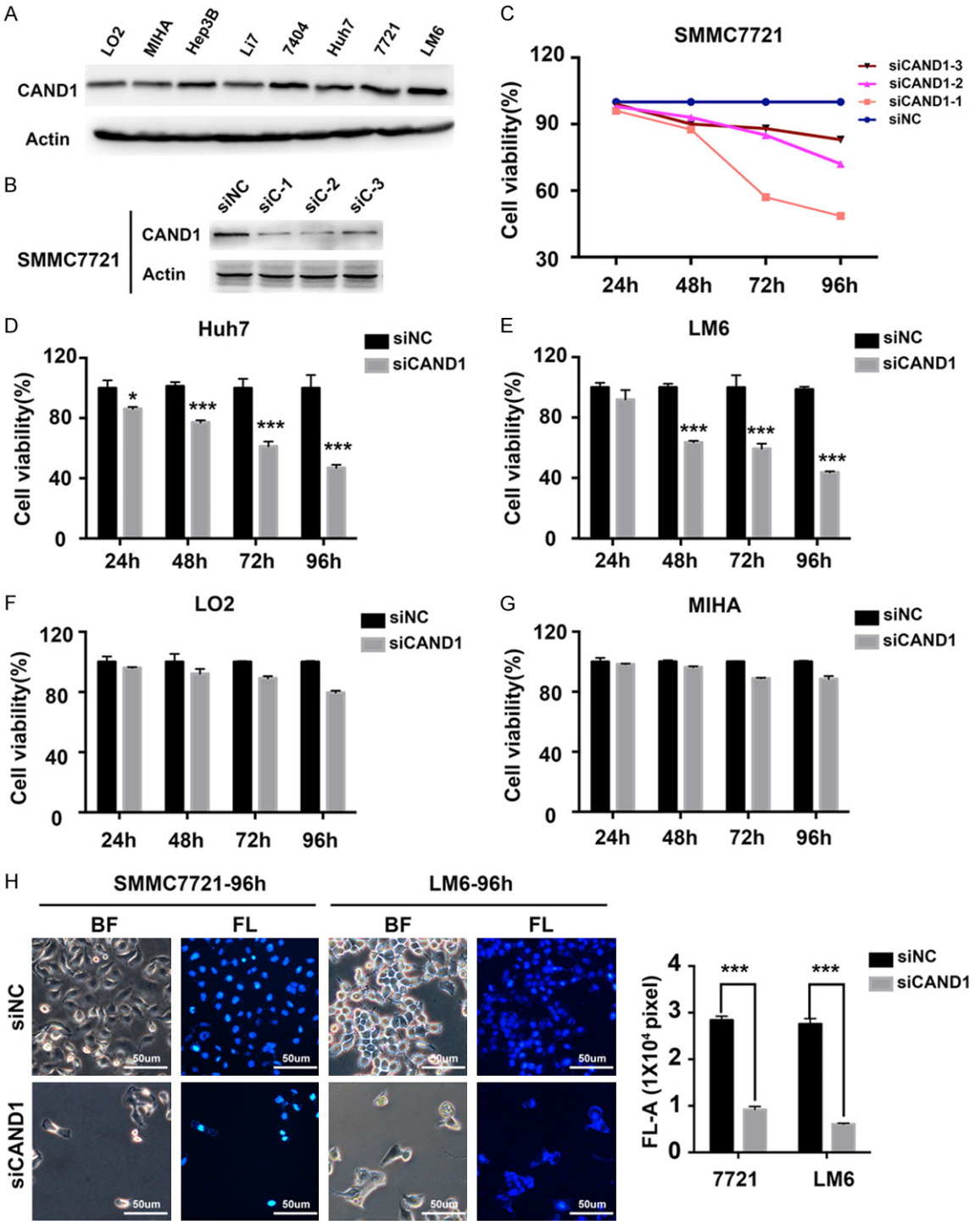

Figure 2. CAND1 knockdown suppressed liver cancer cells proliferation. (A) Western blot showed the expression of CAND1 in immortalized liver cell lines LO2 and MIHA, and in liver cancer cell lines Hep3B, Li7, BEL-7404, Huh7, SMMC7721 (7721) and LM6. (B, C) Three different siRNA sequences were used to confine the expression of CAND1 (siCAND1-1, siCAND1-2 and siCAND1-3). The CAND1 protein level was detected by western blot to confirm the knockdown efficacy in SMMC7721cells treated with siCAND1-1(siC1), siCAND1-2 (siC-2) and siCAND1-3 (siC-3) compared to that of scramble siRNA control (siNC) (B), and the effect of the siRNAs on cell viability was tested by MTS colorimetric assays in SMMC7721 cells (C). (D-G) Cells were transfected with siNC or siCAND1 for 24 h, 48 h, 72 h and 96 h, cell viability was tested by MTS colorimetric assays in Huh7 (D), LM6 (E), LO2 (F) and MIHA (G) (mean ± SD, *P<0.05; ***P<0.001). (H) Hoechst33342 staining was performed 96h after transfection of control or CAND1 siRNAs in SMMC7721 and LM6 cells. The left panel showed the bright field (BF) image and fluorescence (FL) image of the same view in the siCAND1 treatment group and siNC treatment group. The cartogram (right panel) indicated the fluorescence intensity of Hoechst33342 staining. BF: bright field; FL: fluorescence; FL-A: fluorescence area. (mean ± SD, ***P<0.001).

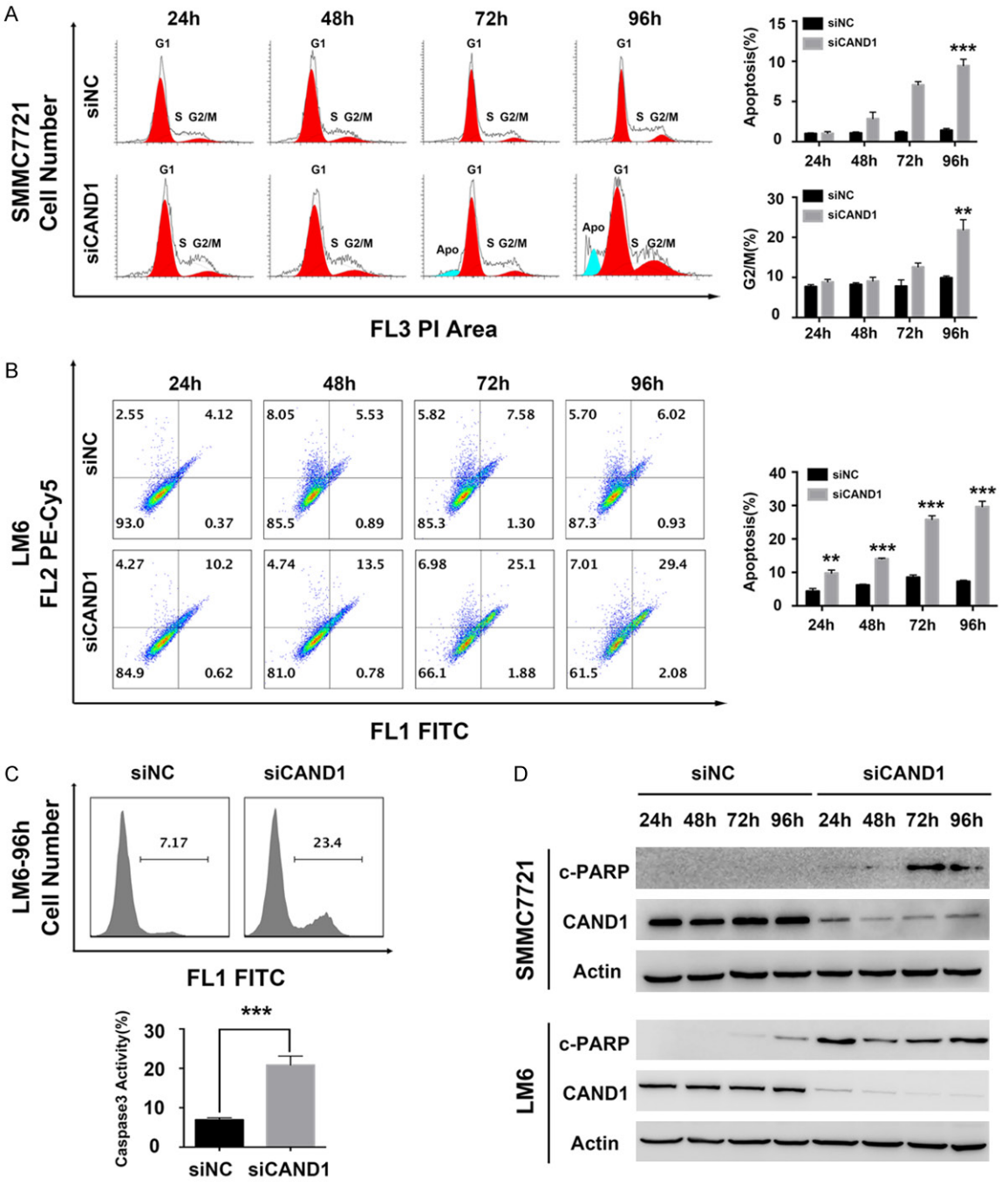

Figure 3. CAND1 knockdown induced apoptosis in HCC cells. A. SMMC7721 cells transfected with siNC or siCAND1 were subjected to cell cycle distribution analysis. The left panel shows the flow charts in the cells treated with either siCAND1 or siNC for the indicated hours. The right panel is the quantitative data for the population of cells at sub-G1 phase, and the population of cells at G2/M phase. (mean ± SD, **P<0.01; ***P<0.001). B. Annexin V and PI staining was used to analyze the apoptotic state of LM6 cells. The total portion of the early apoptotic cells [Annexin V (+) and PI (-)] and the late apoptotic cells [Annexin V (+) and PI (+)] was counted to plot the cartogram. (mean ± SD, **P<0.01; ***P<0.001). C. Capase-3 activation was detected using FITC-DEVD-FMK staining following flow cytometry analysis. The upper panel shows the flow charts in LM6 cells treated with either siCAND1 or siNC for 96 h, respectively; the lower panel is the quantitative data for the upper panel. (mean ± SD, ***P<0.001). D. The expression of apoptotic protein, cleaved-PARP (c-PARP) in SMMC7721 and LM6, was analyzed by western blot with specific antibodies as indicated. β-actin was also detected by western blot as a loading control.

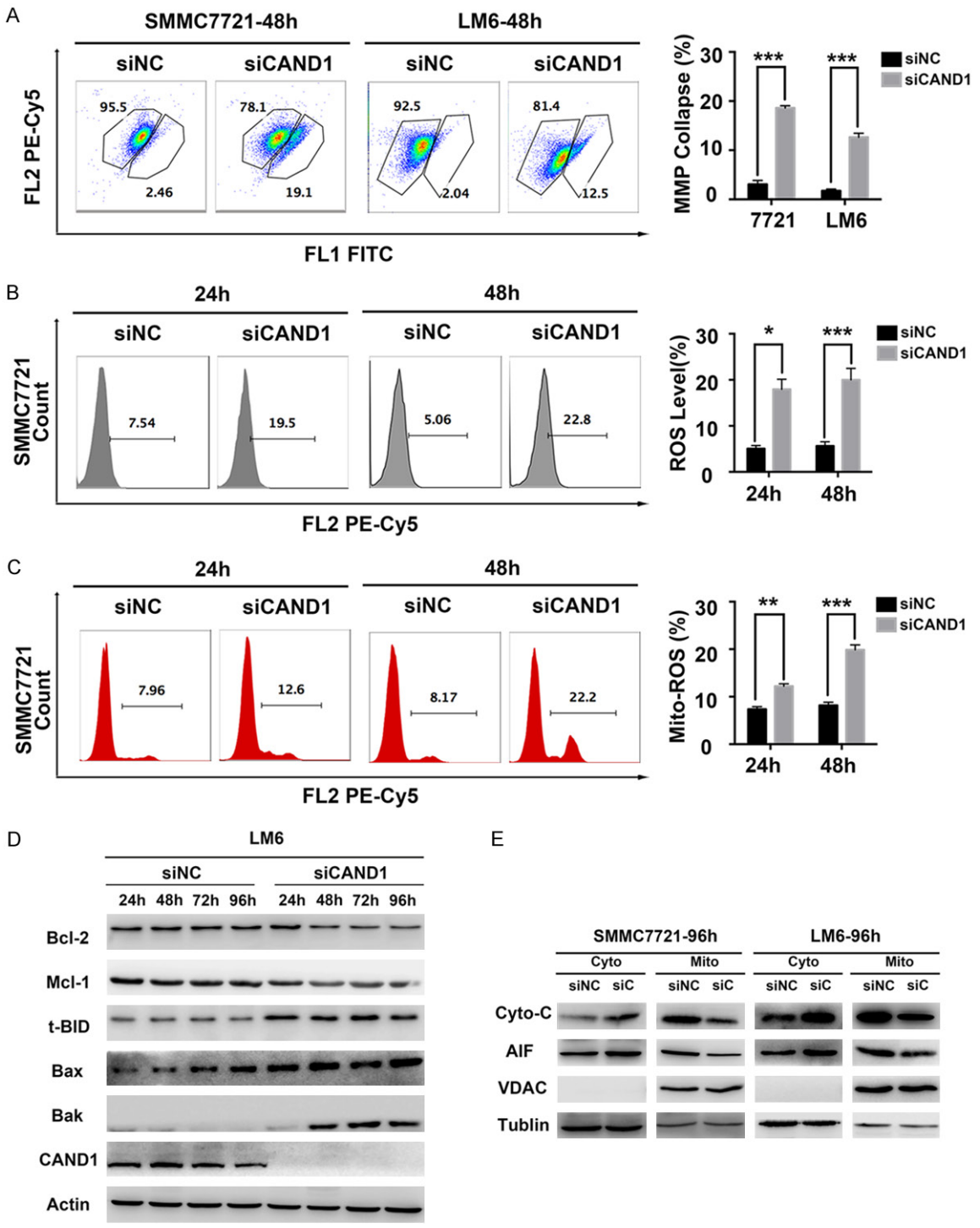

Figure 4. CAND1 knockdown activated mitochondrial apoptotic signal in HCC cells. Liver cancer cell lines SMMC7721 and LM6 were transfected with siNC or siCAND1, respectively. A. Mitochondrial membrane potentials (MMP) collapse in SMMC7721 and LM6 were monitored by JC-1 assays. The left panel shows the flow charts of the cells treated with either siCAND1 or siNC, respectively. The right panel showed the quantitative data in the bar figure. MMP: mitochondrial membrane potential; 7721: SMMC7721 cells. (Mean ± SD, ***P<0.001). B. Intracellular ROS levels were determined using DCFH-DA staining following flow cytometry analysis. The left panel shows the flow charts of the DCFH-DA staining in SMMC7721 cells treated with either siNC or siCAND1 for 24 h and 48 h. The right panel is the quantitative data for the left panel. (mean ± SD, *P<0.05; ***P<0.001). C. Mitochondrial ROS levels were determined using Mito-SOX Red staining following flow cytometry analysis. The left panel showed the flow charts of the Mito-SOX Red staining in SMMC7721 cells treated with either siNC or siCAND1 for 24 h and 48 h. The right panel is the quantitative data for the left panel (mean ± SD, **P<0.01; ***P<0.001). D. The expression of

Bcl-2 family members (Bcl-2, Mcl-1, t-BID, Bax, Bak) was analyzed by western blot in LM6 cells treated with either siNC or siCAND1 for the indicated hours. β-actin was used as a loading control. E. The mitochondrial and cytoplasm gradients were isolated by gradient centrifugation. Apoptotic factors (AIF) released from the mitochondria (Mito) to the cytoplasm (Cyto) were analyzed by Western blot in the cells treated with either siNC or siCAND1 for 96 h. VDAC1 was used as a loading control for mitochondrial gradient; β-Tubulin was used as a loading control for cytoplasm gradient. siC: siCAND1. Cyto-C: cytochrome C. VDAC1: Voltage-Dependent Anion Channel 1.

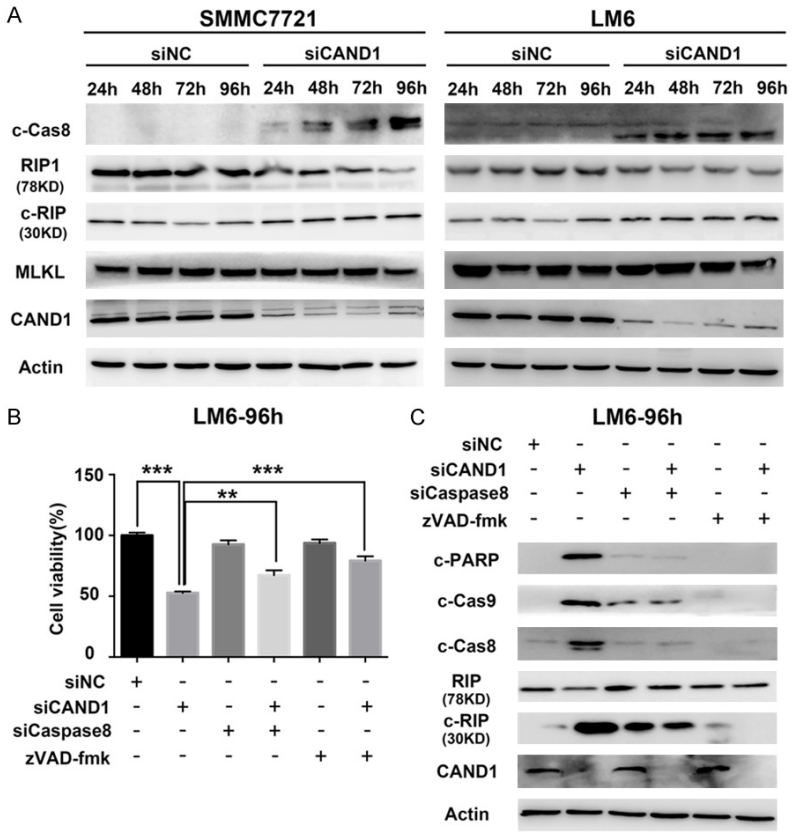

Figure 5. CAND1 knockdown induced caspase-8-dependent cleavage of RIP1. (A) Liver cancer cells were transfected with siControl or siCAND1 for 24 h, 48 h, 72 h, and 96 h. The protein levels for cleavage of Caspase-8 (c-Cas8), RIP protein (RIP 78 KD), cleavage of RIP (c-RIP 30 KD), MLKL and CAND1were analyzed by western blot in the SMMC7721 and LM6 cells treated with either siNC or siCAND1 for indicated hours. β-actin was used as a loading control. (B) Percent viable cells were evaluated by the MTS colorimetric assay in the LM6 cells transfected with siNC, siCAND1, siCaspase-8 or pretreated with Z-VAD-fmk (10 uM) and in the combination of siCAND1 with siCaspase8 or pre-treated with Z-VAD-fmk (10 uM) for 96 h. (mean ± SD, **P<0.01; ***P<0.001). (C) The protein levels for c-PARP, c-Cas9, c-Cas8, RIP (78 KD) and c-RIP (30 KD) were analyzed by western blot in the cells treated with the same scheme on (B).

ly over time in LM6 cells but the siNC had no such effect. The quantitative data showed that the percent of apoptotic cells was significantly increased from 24 to 96 hours with siCAND1 treatment versus that of siNC treatment in the cells (**Figure 3B**). We also detected caspase3 activity by staining the cleaved caspase-3 (c-Cas3) with FITC-DEVD-FMK following flow cytometry analysis. The data showed a significant increase of caspase-3 activation in CAND1-silencing cells compared to the siNC control (**Figure 3C**). Furthermore, cleaved-PARP (c-PARP), the marker for PARP activation was also markedly observed by western blot in both SMMC7721 and LM6 cells in 24 to 96 hours after siCAND1 treatment compared to that of the siNC control (**Figure 3D**). Taken together, these data demonstrated that CAND1 silencing induces apoptosis in liver cancer cells.

Given the knowledge that mitochondria are essential organelles in maintaining cell homeostasis as well as in regulating apoptosis, we wondered if mitochondria were involved in CAND1 knockdown-induced apoptosis. To confirm that, we used the fluorescent probe JC-1 to measure the mitochondria membrane potential (MMP). The results indicated that mitochondria depolarization in the cells of the siCAND1-treated group was over six folds higher than that of the control group in SMMC7721 and LM6 tumor cells. The quantitative data showed the difference was significant in both cells (**Figure 4A**). The intracellular overproduction of reactive oxygen species (ROS) is tightly connected with the mitochondrial apoptosis pathway. We explored the change of the ROS in the cells and found that both the total ROS generation (**Figure 4B**) as well as mitochondrial-specific ROS generation (**Figure 4C**) was significantly

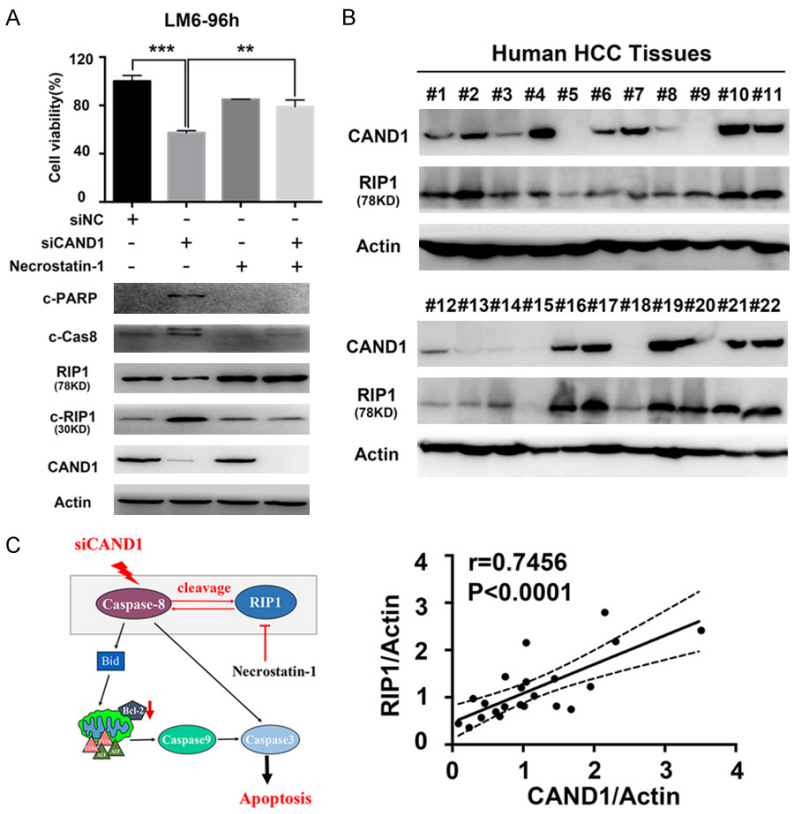

Figure 6. CAND1 knockdown-induced apoptosis was RIP1 kinase activity-dependent. A. LM6 cells were transfected with siCAND1 or pretreated with RIP1 inhibitor Necrostatin-1 (10 uM) for 96 h. Cell viability was analyzed by MTS colorimetric assays and the indicated protein levels were analyzed by western blot. (mean ± SD, **P<0.01; ***P<0.001). B. The protein level of CAND1 and RIP1 in 22 cases of human liver cancer tissues was analyzed by western blot. The upper panel shows the CAND1 and RIP1 protein level in the individual patients. The intensity of RIP and CAND1 level in each patient was also quantitated with a densitometric analysis using the Image J software (MD, USA), and normalized with the intensity of the actin protein in the same patient; the lower panel is the correlation analysis of the normalized RIP1 level and CAND1 level. RIP1/Actin or CAND1/Actin indicated the normalized intensity in each patient. C. Model of CAND1 silencing-induced apoptosis in liver cancer cells.

higher in SMMC7721 cells treated with siCAND1 compared to that of siNC. Statistical analysis showed that the difference of siCAND1 versus siNC in ROS generation was significant (**Figure 4B** and **4C**). The data indicates that the elevated ROS production contributed to the cytotoxicity of CAND1 silencing in liver cancer cells.

Mitochondrial apoptosis is governed by the Bcl-2 family. We observed that siCAND1 treatment for 24 to 96 hours obviously decreased the protein level of anti-apoptotic members Bcl-2 and Mcl-1, while it increased the protein level of apoptotic members Bax and Bak compared to that of siNC treatment (**Figure 4D**). The dysregulation of the Bcl-2 family validated the damage of the mitochondria. Numerous substances inside the mitochondria need to escape into the cytoplasm to trigger the downstream apoptotic signals. We isolated these subcellular fractions and confirmed the release of pro-apoptotic proteins, apoptosis-inducing factor (AIF) and cytochrome-c, from the mitochondria to the cytoplasm upon siCAND1 versus siNC treatment using western blot assays in both SMMC-7721 and LM6 tumor cells (**Figure 4E**). Taken together, these results indicated that CAND1 silencing-induced apoptosis in liver cancer cells is largely dependent on the mitochondrial apoptosis pathway.

CAND1 knockdown induced apoptosis through activation of caspase-8/RIP1 in liver cancer cells

Bid, a bcl-2 member, is normally localized in the cytosolic fraction of cells as an inactive form and when cleaved by caspase-8 leads to transposition of the carboxyl terminal fragment (t-Bid) to the mitochondria outer membrane causing mitochondria damage, and relaying of the apoptotic signals to mitochondria [17]. We found that siCAND1 treatment for 24 to 96 hours also up-regulated the protein level of t-Bid (**Figure 4D**) as well as cleaved-caspase-8 (c-Cas8) (**Figure 5A**) in both SMMC7721 and LM6 tumor cells. These data indicate that caspase-8 may contribute to CAND1 knockdown-induced mitochondrial damage.

To confirm the effect of caspase-8 on CAND1 knockdown-induced apoptosis, LM6 cells were either transfected with caspase-8 siRNA or incubated with the caspase-pan-inhibitor Z-VAD-fmk. We found that either siCaspase-8 or Z-

VAD-fmk treatment could significantly restore siCAND1 induced cell proliferation arrest (**Figure 5B**). The protein levels of cleaved-PARP (c-PARP), and cleaved-caspase-8 (c-Cas8) in the siCAND1 treatment cells were also reduced compared to that of siNC treatment cells upon either siCaspase-8 or Z-VAD-fmk treatment (**Figure 5C**). This data indicates that caspase-8 is required for CAND1 knockdown-induced apoptosis.

Generally, caspase-8 needs to collaborate with other adaptor proteins to form the death inducing signaling complex (DISC) to conduct apoptotic signals [18]. Death domain kinase RIP1, a well-known necroptosis mediator and a DISC complex component, has been suggested to play an important role in the initiation of necroptosis and apoptosis [19, 20]. We showed that siCAND1 treatment for 24 to 96 hours downregulated the protein level of RIP1 (78 KDa) and resulted in an accumulation of cleaved-RIP1 (30 KDa) compared to that of the siNC group in the tumor cells, while it had no effect on the necroptosis effector MLKL (**Figure 5A**). These results supported the notion that RIP1 participates in CAND1 silencing-induced apoptosis. Importantly, when caspase-8 was confined, either by siRNA interference or Z-VAD-fmk pretreatment, the siCAND1-induced cleavage of RIP1 was reversed (**Figure 5C**). These data indicated that caspase-8 mediated the cleavage of RIP1, corresponding to previous reports in the literature [21-23].

Since auto-phosphorylation is critical for RIP1 activation [24-26], we adopted the RIP1 autophosphorylation inhibitor Necrostatin-1 to explore if RIP1 also contributed to CAND1 knockdown-induced apoptosis. Pretreatment of Necrostatin-1 on LM6 cells partially rescued siCAND1-induced proliferation arrest (**Figure 6A**, upper panel) and reversed siCAND1-induced increase of the cleavage of RIP1 (c-RIP1) and cleavage of caspase-8 (c-Cas8) (**Figure 6A**, lower panel). These data supported that RIP1, mainly depending on its kinase activity, induced caspase-8-dependent apoptosis upon CAND1 silencing. We also detected the protein levels of both CAND1 and RIP1 in 22 human liver cancer tissues, and found that CAND1 and RIP1 protein were concurrently detected in the same individual patients (**Figure 6B**, upper two panels). We also quantified the protein level by ImageJ and found that their protein levels were positively correlated ($r=0.7456$, $P<0.0001$) (**Figure 6B**, bottom panel). Taken together, these data show that caspase-8-dependent cleavage of RIP1 in turn promotes the activation of caspase-8 in a RIP1 kinase activity-dependent manner, and the interdependent activation of caspase-8 and RIP1 amplifies CAND1-knockdown-induced apoptotic signals. **Figure 6C** summarizes the molecular mechanism underlying CAND1 silencing induced apoptosis in liver cancer cells, which is also described in detail in the discussion section.

Discussion

Liver cancer is the sixth most common malignancy and causes the second most cancer-related deaths worldwide. HCC patients have poor clinical outcomes owing to rapid progression, high recurrence rate, and limited treatment choices [27, 28]. It is quite urgent to further understand the mechanisms underlying HCC carcinogenesis and identify potential targets for the development of new therapies.

The expression of CAND1 is closely regulated by miRNAs in tumorigenesis. By targeting CAND1, miR-33a inhibits cell proliferation and invasion in lung tumor [29], and miR-148b-3p promotes migration of Schwann cells [30]. CAND1 has also been reported to control the centriole duplication in prostate cancer [31], and contribute to the development of highly aggressive lung tumors [32]. To our best knowledge, the present study first reported that CAND1 was overexpressed in human liver cancer tissues. Our data also indicated that CAND1 expression may serve as an independent predictor for prognosis of liver cancer patients, although this needs to be confirmed with a larger cohort study.

It is reported that CRL E3 ligase mediates proteasomal degradation of numerous proteins, regulating cell cycle progression [33-35]. Owing to the central role in cell cycle control, aberrant expression of the components of CRLs and their regulators is thought to play a role during tumorigenesis. Intriguingly, CAND1 overexpression causes elevation of p27 and promotes adipogenesis, and also cancer development [36-38]. In the current study, we have shown that high expression of CAND1 is positively correlated with tumor differentiation and tumor size

with the pathological association analysis; we also provided solid evidence indicating that CAND1 plays a vital role in regulating HCC cells proliferation and apoptosis. Taken together, our results indicate that the high expression of CAND1 is involved in cell proliferation and differentiation in liver cancer.

Apoptosis is considered a vital component of many biological and pathological processes, while inappropriate apoptosis is involved in tumorigenesis in many kinds of cancers. This makes the apoptotic pathways promising targets for cancer therapy [39, 40]. In the present study, CAND1 knockdown induced obvious apoptosis in liver cancer cell lines SMMC7721 and LM6, while it had little lethal effect on immortalized liver cell lines LO2 and MIHA. Our data showed that CAND1 silencing could selectively kill tumor cells, which reveals the potential of CAND1 as a target for promising therapy in liver cancer.

We also explored the underlying molecular mechanism for siCAND1-induced apoptosis in these cells. CAND1 knockdown induced the activation of caspase-8, and further increased ROS production through regulation of the Bax/Bcl-2 axis to trigger apoptosis (model see **Figure 6C**). The activation of caspase-8 can be initiated at the plasma membrane upon ligation of death receptors. Briefly, once the extrinsic apoptosis was initiated; which was mediated by death receptors; caspase-8 was recruited to the plasma to form the death-inducing signaling complex (DISC) following the auto-activation of caspase-8 [18]. Here is one assumption, although further studies should be performed; CAND1 knockdown results in the dysregulation of CRLs' substrates, including numerous apoptotic-related proteins such as death receptors, and activated extrinsic apoptosis through caspase-8.

RIP1 can be cleaved by caspase-8 at the kinase domain (KD) and intermediate domain (ID) [22]; and by cysteine cathepsins B and S [41]. Caspase-8-mediated cleavage of RIP1 resulted in cell death induction in response to TNF and TRAIL [22, 42]. These reports indicate that caspase-8-mediated cleavage of RIP1 can be initiated in response to different signals. Importantly, RIP1 has been suggested to activate caspase-8 through a RIP1-Fas-associated death domain protein scaffold to promote apoptosis [43, 44], while A20 ubiquitin ligase-mediated polyubiquitination of RIP1 inhibited the activation of caspase-8 in glioblastoma [45]. This suggests that RIP1 participated in the regulation of caspase-8 activation. In this study, CAND1 knockdown leads to caspase-8-mediated cleavage of RIP1, and the activated RIP1 promotes the activation of caspase-8 in turn. Moreover, treatment of the RIP1 kinase inhibitor necrostatin-1 reversed the activation of caspase-8. These data also indicated that CAND1 silencing-induced apoptosis is caspase-8 and RIP1 kinase activity dependent; in other words, caspase-8 and RIP1 are mutually activated by each other to amplify the apoptotic signals in CAND1-silencing cells (mutual activation loop, **Figure 6C**).

In our study, a positive correlation between the protein level of CAND1 and RIP1 in human liver cancer tissues was observed. Although the specific mechanism needs to be further clarified, we assumed that CAND1 collaborating with RIP1 promoted liver cancer cells survival. Our future work will follow the relevance and significance of these two molecules in liver cancer.

In summary, this study represents the first report of high CAND1 expression as a poor prognostic factor in liver cancer patients. CAND1 knockdown suppresses the proliferation of liver cancer cells through induction of apoptosis with a caspase-8/RIP1 dependent mechanism. Our data may be proof for the potential value of targeting CAND1 as a therapeutic strategy in HCC.

Acknowledgements

This work was supported by the grant of the National Natural Science Foundation of China to Dongqin Yang (81572336, 81372652), and jointly by the Development Found for Shanghai Talents (201660).

Disclosure of conflict of interest

None.

Address correspondence to: Dr. Dongqin Yang, Department of Digestive Diseases, Huashan Hospital, Fudan University, Shanghai 200040, China. Tel: 86-21-52888234; Fax: 86-21-52888236; E-mail: yangdongqin@huashan.org.cn

References

[1] Sarikas A, Hartmann T and Pan ZQ. The cullin protein family. Genome Biol 2011; 12: 220.

[2] Petroski MD and Deshaies RJ. Function and regulation of cullin-RING ubiquitin ligases. Nat Rev Mol Cell Biol 2005; 6: 9-20.

[3] Zhao Y and Sun Y. Cullin-RING Ligases as attractive anti-cancer targets. Curr Pharm Des 2013; 19: 3215-3225.

[4] Nakayama KI and Nakayama K. Ubiquitin ligases: cell-cycle control and cancer. Nat Rev Cancer 2006; 6: 369-381.

[5] Schmidt MW, McQuary PR, Wee S, Hofmann K and Wolf DA. F-box-directed CRL complex assembly and regulation by the CSN and CAND1. Mol Cell 2009; 35: 586-597.

[6] Enchev RI, Schulman BA and Peter M. Protein neddylation: beyond cullin-RING ligases. Nat Rev Mol Cell Biol 2015; 16: 30-44.

[7] Lydeard JR, Schulman BA and Harper JW. Building and remodelling Cullin-RING E3 ubiquitin ligases. EMBO Rep 2013; 14: 1050-1061.

[8] Soucy TA, Smith PG, Milhollen MA, Berger AJ, Gavin JM, Adhikari S, Brownell JE, Burke KE, Cardin DP, Critchley S, Cullis CA, Doucette A, Garnsey JJ, Gaulin JL, Gershman RE, Lublinsky AR, McDonald A, Mizutani H, Narayanan U, Olhava EJ, Peluso S, Rezaei M, Sintchak MD, Talreja T, Thomas MP, Traore T, Vyskocil S, Weatherhead GS, Yu J, Zhang J, Dick LR, Claiborne CF, Rolfe M, Bolen JB and Langston SP. An inhibitor of NEDD8-activating enzyme as a new approach to treat cancer. Nature 2009; 458: 732-736.

[9] Abidi N and Xirodimas DP. Regulation of cancer-related pathways by protein NEDDylation and strategies for the use of NEDD8 inhibitors in the clinic. Endocr Relat Cancer 2015; 22: T55-70.

[10] Sarantopoulos J, Shapiro GI, Cohen RB, Clark JW, Kauh JS, Weiss GJ, Cleary JM, Mahalingam D, Pickard MD, Faessel HM, Berger AJ, Burke K, Mulligan G, Dezube BJ and Harvey RD. Phase I Study of the Investigational NEDD8-activating enzyme inhibitor pevonedistat (TAK-924/MLN4924) in patients with advanced solid tumors. Clin Cancer Res 2016; 22: 847-857.

[11] Shah JJ, Jakubowiak AJ, O'Connor OA, Orlowski RZ, Harvey RD, Smith MR, Lebovic D, Diefenbach C, Kelly K, Hua Z, Berger AJ, Mulligan G, Faessel HM, Tirrell S, Dezube BJ and Lonial S. Phase I Study of the Novel Investigational NEDD8-activating enzyme inhibitor pevonedistat (MLN4924) in patients with relapsed/refractory multiple myeloma or lymphoma. Clin Cancer Res 2016; 22: 34-43.

[12] Yang D, Li L, Liu H, Wu L, Luo Z, Li H, Zheng S, Gao H, Chu Y, Sun Y, Liu J and Jia L. Induction of autophagy and senescence by knockdown of ROC1 E3 ubiquitin ligase to suppress the growth of liver cancer cells. Cell Death Differ 2013; 20: 235-247.

[13] Lv B, Song C, Wu L, Zhang Q, Hou D, Chen P, Yu S, Wang Z, Chu Y, Zhang J, Yang D and Liu J. Netrin-4 as a biomarker promotes cell proliferation and invasion in gastric cancer. Oncotarget 2015; 6: 9794-9806.

[14] Liu F, Wang G, Wang X, Che Z, Dong W, Guo X, Wang Z, Chen P, Hou D, Zhang Q, Zhang W, Pan Y, Yang D and Liu H. Targeting high Aurora kinases expression as an innovative therapy for hepatocellular carcinoma. Oncotarget 2017; 8: 27953-27965.

[15] Zhang Q, Hou D, Luo Z, Chen P, Lv B, Wu L, Ma Y, Chu Y, Liu H, Liu F, Yu S, Zhang J, Yang D and Liu J. The novel protective role of P27 in MLN4924-treated gastric cancer cells. Cell Death Dis 2015; 6: e1867.

[16] Yu S, Hou D, Chen P, Zhang Q, Lv B, Ma Y, Liu F, Liu H, Song EJ, Yang D and Liu J. Adenosine induces apoptosis through TNFR1/RIPK1/P38 axis in colon cancer cells. Biochem Biophys Res Commun 2015; 460: 759-765.

[17] Cosentino K and Garcia-Saez AJ. Mitochondrial alterations in apoptosis. Chem Phys Lipids 2014; 181: 62-75.

[18] Dickens LS, Boyd RS, Jukes-Jones R, Hughes MA, Robinson GL, Fairall L, Schwabe JW, Cain K and Macfarlane M. A death effector domain chain DISC model reveals a crucial role for caspase-8 chain assembly in mediating apoptotic cell death. Mol Cell 2012; 47: 291-305.

[19] Nikoletopoulou V, Markaki M, Palikaras K and Tavernarakis N. Crosstalk between apoptosis, necrosis and autophagy. Biochim Biophys Acta 2013; 1833: 3448-3459.

[20] Wu XN, Yang ZH, Wang XK, Zhang Y, Wan H, Song Y, Chen X, Shao J and Han J. Distinct roles of RIP1-RIP3 hetero- and RIP3-RIP3 homo-interaction in mediating necroptosis. Cell Death Differ 2014; 21: 1709-1720.

[21] Rajput A, Kovalenko A, Bogdanov K, Yang SH, Kang TB, Kim JC, Du J and Wallach D. RIG-I RNA helicase activation of IRF3 transcription factor is negatively regulated by caspase-8-mediated cleavage of the RIP1 protein. Immunity 2011; 34: 340-351.

[22] Zhang L, Blackwell K, Workman LM, Chen S, Pope MR, Janz S and Habelhah H. RIP1 cleavage in the kinase domain regulates TRAIL-induced NF-kappaB activation and lymphoma survival. Mol Cell Biol 2015; 35: 3324-3338.

[23] Lin Y, Devin A, Rodriguez Y and Liu ZG. Cleavage of the death domain kinase RIP by caspase-8 prompts TNF-induced apoptosis. Genes Dev 1999; 13: 2514-2526.

[24] Cho YS, Challa S, Moquin D, Genga R, Ray TD, Guildford M and Chan FK. Phosphorylation-driven assembly of the RIP1-RIP3 complex regulates programmed necrosis and virus-induced inflammation. Cell 2009; 137: 1112-1123.
[25] Christofferson DE, Li Y and Yuan J. Control of life-or-death decisions by RIP1 kinase. Annu Rev Physiol 2014; 76: 129-150.
[26] McQuade T, Cho Y and Chan FK. Positive and negative phosphorylation regulates RIP1- and RIP3-induced programmed necrosis. Biochem J 2013; 456: 409-415.
[27] Huang MA and Marrero JA. Hepatocellular carcinoma. Curr Opin Gastroenterol 2002; 18: 345-350.
[28] Bruix J, Reig M and Sherman M. Evidence-based diagnosis, staging, and treatment of patients with hepatocellular carcinoma. Gastroenterology 2016; 150: 835-853.
[29] Kang M, Li Y, Zhao Y, He S and Shi J. miR-33a inhibits cell proliferation and invasion by targeting CAND1 in lung cancer. Clin Transl Oncol 2017; [Epub ahead of print].
[30] Qian TM, Zhao LL, Wang J, Li P, Qin J, Liu YS, Yu B, Ding F, Gu XS and Zhou SL. miR-148b-3p promotes migration of Schwann cells by targeting cullin-associated and neddylation-dissociated 1. Neural Regen Res 2016; 11: 1001-1005.
[31] Korzeniewski N, Hohenfellner M and Duensing S. CAND1 promotes PLK4-mediated centriole overduplication and is frequently disrupted in prostate cancer. Neoplasia 2012; 14: 799-806.
[32] Salon C, Brambilla E, Brambilla C, Lantuejoul S, Gazzeri S and Eymin B. Altered pattern of Cul-1 protein expression and neddylation in human lung tumours: relationships with CAND1 and cyclin E protein levels. J Pathol 2007; 213: 303-310.
[33] Frescas D and Pagano M. Deregulated proteolysis by the F-box proteins SKP2 and beta-TrCP: tipping the scales of cancer. Nat Rev Cancer 2008; 8: 438-449.
[34] Matsumoto A, Onoyama I, Sunabori T, Kageyama R, Okano H and Nakayama KI. Fbxw7-dependent degradation of Notch is required for control of "stemness" and neuronal-glial differentiation in neural stem cells. J Biol Chem 2011; 286: 13754-13764.
[35] Bashir T, Dorrello NV, Amador V, Guardavaccaro D and Pagano M. Control of the SCF(Skp2-Cks1) ubiquitin ligase by the APC/C(Cdh1) ubiquitin ligase. Nature 2004; 428: 190-193.
[36] Dubiel D, Gierisch ME, Huang X, Dubiel W and Naumann M. CAND1-dependent control of cullin 1-RING Ub ligases is essential for adipogenesis. Biochim Biophys Acta 2013; 1833: 1078-1084.
[37] Dubiel D, Ordemann J, Pratschke J, Dubiel W and Naumann M. CAND1 exchange factor promotes Keap1 integration into cullin 3-RING ubiquitin ligase during adipogenesis. Int J Biochem Cell Biol 2015; 66: 95-100.
[38] Tikhmyanova N, Tutton S, Martin KA, Lu F, Kossenkov AV, Paparoidamis N, Kenney S, Salvino JM and Lieberman PM. Small molecule perturbation of the CAND1-Cullin1-ubiquitin cycle stabilizes p53 and triggers Epstein-Barr virus reactivation. PLoS Pathog 2017; 13: e1006517.
[39] Ashkenazi A, Fairbrother WJ, Leverson JD and Souers AJ. From basic apoptosis discoveries to advanced selective BCL-2 family inhibitors. Nat Rev Drug Discov 2017; 16: 273-284.
[40] Roos WP, Thomas AD and Kaina B. DNA damage and the balance between survival and death in cancer biology. Nat Rev Cancer 2016; 16: 20-33.
[41] McComb S, Shutinoski B, Thurston S, Cessford E, Kumar K and Sad S. Cathepsins limit macrophage necroptosis through cleavage of Rip1 kinase. J Immunol 2014; 192: 5671-5678.
[42] Yang S, Wang B, Tang LS, Siednienko J, Callanan JJ and Moynagh PN. Pellino3 targets RIP1 and regulates the pro-apoptotic effects of TNF-alpha. Nat Commun 2013; 4: 2583.
[43] Abhari BA, Cristofanon S, Kappler R, von Schweinitz D, Humphreys R and Fulda S. RIP1 is required for IAP inhibitor-mediated sensitization for TRAIL-induced apoptosis via a RIP1/FADD/caspase-8 cell death complex. Oncogene 2013; 32: 3263-3273.
[44] Feoktistova M, Geserick P, Kellert B, Dimitrova DP, Langlais C, Hupe M, Cain K, MacFarlane M, Hacker G and Leverkus M. cIAPs block Ripoptosome formation, a RIP1/caspase-8 containing intracellular cell death complex differentially regulated by cFLIP isoforms. Mol Cell 2011; 43: 449-463.
[45] Bellail AC, Olson JJ, Yang X, Chen ZJ and Hao C. A20 ubiquitin ligase-mediated polyubiquitination of RIP1 inhibits caspase-8 cleavage and TRAIL-induced apoptosis in glioblastoma. Cancer Discov 2012; 2: 140-155.